frontiers | Frontiers in Earth Science

TYPE Original Research
PUBLISHED 14 October 2025
DOI 10.3389/feart.2025.1698922

OPEN ACCESS

EDITED BY
Binbin Yang,
Xuchang University, China

REVIEWED BY
Shuang Shu,
Hohai University, China
Fanyan Meng,
Hunan University of Traditional Chinese Medicine, China

*CORRESPONDENCE
Bo Yang,
yangbo@haut.edu.cn

RECEIVED 04 September 2025
ACCEPTED 30 September 2025
PUBLISHED 14 October 2025

CITATION
Yang B, Chen S, Zhang C, Su N, Zhang S and Zhu D (2025) Experimental study on buoyancy and side friction of underground silos in sand and silty clay.
Front. Earth Sci. 13:1698922.
doi: 10.3389/feart.2025.1698922

Experimental study on buoyancy and side friction of underground silos in sand and silty clay

Bo Yang[1]*, Shaopeng Chen[1], Chengyao Zhang[2], Na Su[3], Shun Zhang[1] and Di Zhu[1]

[1]School of Civil Engineering, Henan University of Technology, Zhengzhou, China, [2]Center International Group Co., Ltd., Beijing, China, [3]Department of Civil Engineering, Central South University, Changsha, China

In current anti-flotation designs for underground structures, buoyancy is typically calculated based on Archimedes' principle and the contribution of side friction is often neglected, potentially resulting in unnecessary construction costs. In this study, a silo model with a vertically movable base was designed to conduct buoyancy tests under various water levels in both sand and silty clay. The attenuation pattern of groundwater buoyancy was analyzed, and the contribution of side friction to anti-flotation performance was also evaluated. The results indicate that: (1) Under the same water level, pore water pressure in sand was generally higher than that in silty clay, and with faster transmission and stabilization. (2) Buoyancy in sand was typically larger than that in silty clay at identical water level. Corresponding to the water levels of 65 cm, 70 cm, and 75 cm, the reduction coefficients of buoyancy were 0.87, 0.93, and 0.98 in sand, and 0.82, 0.89, and 0.94 in silty clay respectively. (3) The side friction acting on the silo model in sand was consistently lower than that in silty clay. The ratios of side friction to theoretical buoyancy in sand were 0.35, 0.32, and 0.25 at the water levels of 65 cm, 70 cm, and 75 cm, respectively; while in silty clay, the corresponding values were 0.47, 0.41, and 0.34. In practical engineering, it might be more rational to consider the reduction of buoyancy and the contribution of side friction, especially in weakly permeable soils such as silty clay, in the anti-flotation design of underground structures.

KEYWORDS

underground silo, buoyancy, side friction, pore water pressure, reduction coefficient

1 Introduction

Grain storage facilities are essential infrastructure for ensuring food security and people's livelihood (Jiang and Guo, 2017). At present, grain is primarily stored in aboveground facilities such as flat warehouses, squat silos, and vertical silos (Wang et al., 2013). The disadvantages of these aboveground grain storage facilities, such as high internal temperatures, large land occupation, excessive energy consumption, and poor grain quality, are increasingly in conflict with the emerging development ideas of green, low-carbon, energy-efficient, and environmentally friendly practices (Yuan et al., 2025a). Thus, it is of significant advantages over traditional aboveground grain storage methods to utilize naturally low-temperature and enclosed conditions of the underground environment to construct subsurface

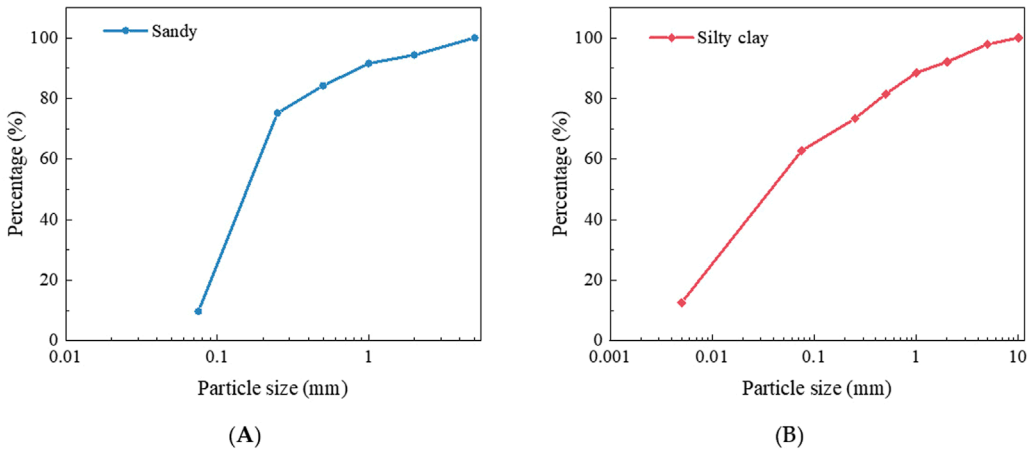

FIGURE 1
Particle size distribution curves of the soils: **(A)** Sand, **(B)** Silty clay.

TABLE 1 Physical and mechanical properties of the soil samples.

Soil parameters	Sand	Silty clay	Testing method
Internal friction angle (°)	37.90	17.40	Direct shear test
Cohesion (kPa)	—	38.83	
Water content (%)	15	18.4	Drying method
Specific gravity	2.65	2.72	Pycnometer method
Maximum dry density (g/cm^3)	1.73	1.78	Sand: Vibration hammering method Silty clay: Compaction test
Minimum dry density (g/cm^3)	1.28	—	Measuring cylinder method
Optimal moisture content (%)	—	23.35	Compaction test
Liquid limit (%)	—	36.01	Limit water content test
Plastic limit (%)	—	23.86	
Plasticity index	—	12.15	
Friction coefficients between soil and cement mortar	0.38	0.49	Inclined plane sliding test method Cui et al. (1999)

storage facilities (Hu et al., 2013). Based on the unique advantages of underground grain storage, large-scale underground circular silos made of reinforced concrete for bulk grain storage have been developed and constructed over the past 20 years in China.

Underground silos, as special large-scale underground structures, are subjected to groundwater buoyancy during both construction and operation stages, and its anti-floating safety need to be paid attention to. Extensive research has been conducted by relevant scholars on the calculation of buoyancy acting on underground structures. Mu et al. (2019) conducted laboratory model tests to investigate the variation of pore water pressure in homogeneous soil layers under different hydraulic gradients, as well as in weakly permeable layers subjected to confined water flow. Liang et al. (2024) carried out model tests to analyze the variation of uplift force on underground structures in weak permeability soils, and found that the buoyancy reduction coefficient ranged from approximately 0.9–0.94 in remolded loess and from 0.82 to 0.88 in silty clay. Based on experimental studies on sand and clay, Zhang (2007) pointed out that the buoyancy acting on underground structures should be calculated using the full hydraulic head, and the reduction coefficient should not be set lower than 0.9. With laboratory-scale model tests, Gao et al. (2025) discovered that the reduction slope of the fitted line between the static water head in the silty clay and the buoyancy water head was 0.87. Ren et al. (2022)

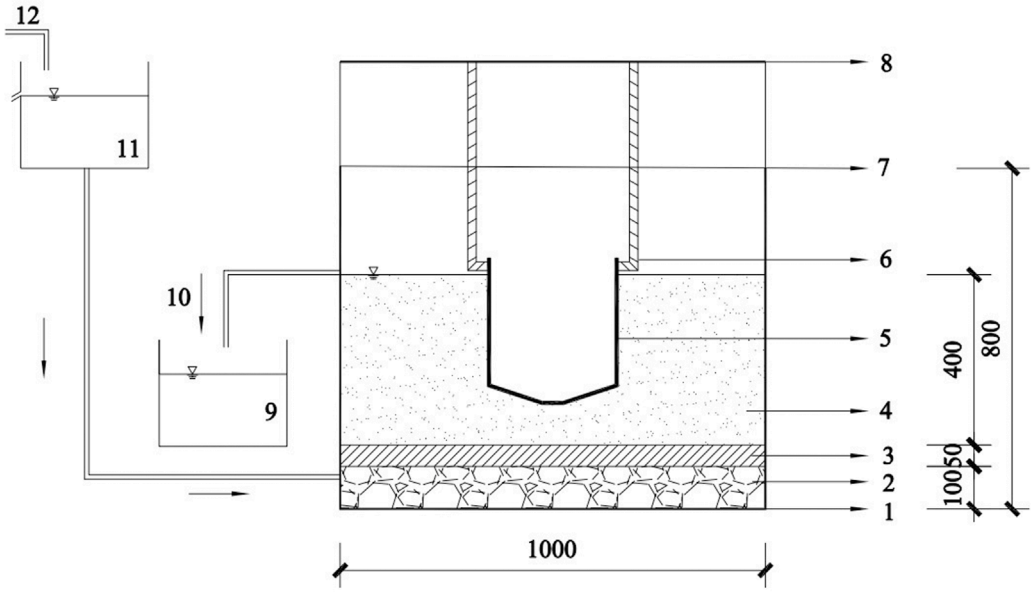

FIGURE 2
Schematic cross-section of the model test setup: 1. Model pool, 2. Crushed stone, 3. Coarse sand, 4. Backfilling soil, 5. Underground silo model, 6. Height adjustment device, 7. Angle steel, 8. Constrained crossbar, 9. Catch pool, 10. Water outlet pipe, 11. Water supply pool, 12. Water supply pipe.

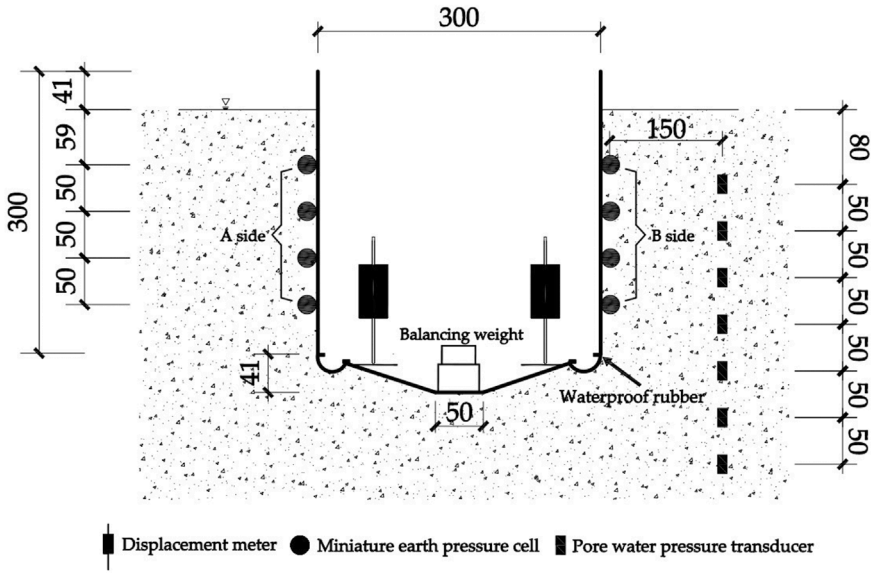

FIGURE 3
Layout of sensors sectional drawing (unit: mm).

performed laboratory experiments to measure the time-dependent variation of the buoyancy reduction coefficient and found that the initial coefficient ranged from approximately 0.55–0.66, gradually increasing to 0.82 over time and eventually stabilizing. Zhang et al. (2019) utilized model tests to evaluate buoyancy of underground silos in sand and clay and the results showed that the buoyancy reduction coefficient of was 0.95 in saturated coarse sand and 0.79 in low-permeability clay. Existing studies show differing opinions on whether buoyancy should be reduced and to what extent in soils, particularly in weakly permeable soils such as clay.

In complex geological conditions, vertical seepage of groundwater is prone to alter the effective stress within the soil, thereby affecting the accurate estimation of lateral earth pressure (Song et al., 2018). Regarding the friction coefficient at the interface between the outer walls of underground structures and the surrounding soil, researchers have determined this parameter

TABLE 2 Sensor parameters.

Sensor category	Measuring range	Accuracy
Displacement meter	±25 mm	0.001 mm
Pore water pressure transducer	−10~50 kPa	0.01 kPa
Miniature earth pressure cell	0~50 kPa	0.01 kPa

TABLE 3 Test conditions.

Test condition	Soil type	Groundwater level/(cm)
S_{75}	Sand	75
S_{70}		70
S_{65}		65
C_{75}	Silty clay	75
C_{70}		70
C_{65}		65

through laboratory inclined plane tests (Cui et al., 1999) and large-scale direct shear tests (Han et al., 2009). The results indicated that the friction coefficient is closely related to factors such as soil type, density, moisture content, and the surface roughness of the structural walls (Zhou, 2015; Guo et al., 2021; Wang et al., 2022; Zhao et al., 2022). According to the results of static cone penetration tests, the ultimate side resistance of enclosure structure of the subway station was calculated and the relationship between side friction resistance in anti-floating design and ultimate side resistance proposed (Ye and Liu, 2010). Li et al. (2020) employed centrifuge model tests and numerical simulation to analyze the role of side friction resistance in counteracting buoyancy forces on large-scale underground liquefied natural gas storage tanks in standard sand. Tang et al. (2013) conducted model tests to derive calculation formulas for side friction in various soil layers and their effects on buoyancy forces acting on structure models. Liu et al. (2021) performed water injection tests to investigate the effect of silo diameter and backfill soil type on the variation of groundwater buoyancy and sidewall friction during both the stationary and uplift stages of the model.

In summary, current anti-floating designs for underground structures typically calculate buoyancy based on Archimedes' principle and neglect the contribution of sidewall friction, which often leads to overly conservative designs, resulting in higher construction costs and unnecessary resource consumption. In this study, a cylindrical model with a vertically movable truncated conical base was designed and buoyancy model tests were conducted in sand and silty clay under different water level conditions to analyze the reduction pattern of groundwater buoyancy and to evaluate the contribution of side friction to anti-floating performance. The results are expected to provide theoretical support and technical guidance for the optimization of anti-uplift design in underground structures.

2 Materials and methods

2.1 Soils

The sand and silty clay required for this study were sampled from a foundation pit in Zhengzhou, Henan Province, China. The physical and mechanical properties of the sand and silty clay were tested in accordance with the Standard for Soil Test Methods (GB/T 50123-2019). The particle size distribution curves of the 2 soils are shown in Figure 1, and their basic physical and mechanical properties are listed in Table 1.

In addition, to investigate the influence of side friction, the friction coefficients between the 2 types of soil and cement mortar were measured using the inclined plane sliding test method, as proposed by Cui et al. (1999). The specific procedure is as follows: Place the cutting ring holding the soil sample upside down on a flat plate coated with mortar identical to that used on the outer walls of the silo model, ensuring the soil sample slightly protrudes beyond edge of the cutting ring. Gradually lift one end of the plate until the soil begins to slide. At this moment, the soil sample is in a state of critical sliding. Thus, the sliding force is the downward component of gravity along the plate and is equal to the frictional resistance. Record the lift height of the end at this moment and calculate the angle between the flat plate and the horizontal plane. The friction coefficient between soil and cement mortar could be obtained by averaging the tangent values of the angles from several trials according to the basic principle of statics. The test results are also listed in Table 1.

2.2 Test equipment

The model tests setup (Figure 2) is mainly consisted of a model pool, an underground silo model, and a data acquisition system.

The model pool, with a side length of 1000 mm and height of 800 mm, are fabricated with 5 mm thick tempered glass. 2 holes are respectively bored at the heights of 55 cm and 10 cm to the bottom to serve as water outlet and inlet. A circumferential water pipe is laid at the bottom, with holes drilled every 10 cm along the pipe to facilitate the vertical seepage of water. A 10 cm gravel layer is placed at the very bottom, covered with a 200mesh filter mesh to prevent soil particles from clogging the outlet holes. Above the filter mesh, a 5 cm layer of coarse sand is arranged to simulate a permeable layer in actual geological conditions. The backfilling soil layer (either sand or silty clay) with a thickness of 40 cm is placed above the coarse sand.

A silo model was fabricated from polypropylene (PP) at a scale of 1:80 based on the actual dimensions of an underground silo (Zhang et al., 2024). The silo model was consisted of a cylindrical wall section with a mass of 3 kg and a truncated conical bottom section with a mass of 1.2 kg. The silo bottom was connected to the wall using waterproof rubber combined with metal press strips, forming a vertically movable bottom structure within a certain range. Thus, the influence of sidewall friction (Liu and

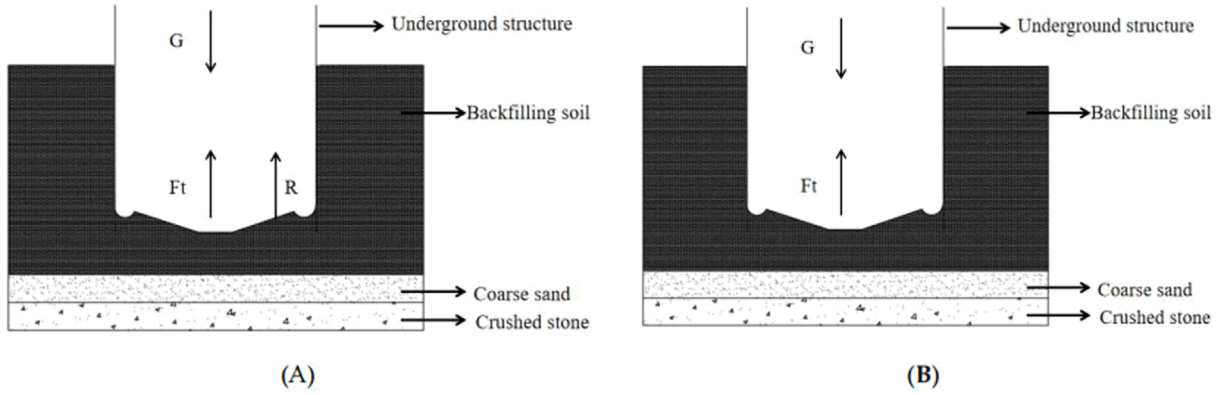

FIGURE 4
Schematic diagram of forces acting on the underground structure: **(A)** Before floating; **(B)** Floating moment.

Wan, 2020) and bottom adsorption could be eliminated and the buoyancy force could be measured accurately during the uplift of the bottom (Zhang et al., 2019). In addition, the outer wall of the silo model was uniformly coated with cement mortar to simulate the contact conditions between the actual underground silo and the surrounding soil.

The data acquisition system was consisted of displacement meter, pore water pressure transducers, miniature earth pressure cells, and a static strain acquisition instrument. 2 displacement meters, numbered as A and B, were symmetrically installed on the model baseplate to monitor the displacement of the model bottom. Seven pore water pressure transducers, with a vertical spacing of 5 cm, were buried in the backfilling soil to monitor pore water pressure at different depths. Eight miniature earth pressure cells were equally divided into 2 groups and symmetrically attached to the outer surface of the model wall with a vertical spacing of 5 cm also. The detailed arrangement of the displacement meters, miniature earth pressure cells, and pore water pressure transducers is shown in Figure 3, and the specifications are listed in Table 2.

2.3 Procedure of test

Six test conditions were designed based on soil type and groundwater level and summarized in Table 3.

Note: The water level is measured from the bottom of the backfilling soil.

The operational procedures of the 6 test conditions were slightly different. Here, the buoyancy test of the underground structure in sand is taken as an example for illustration.

1. Before the test, crushed stone, filter mesh and coarse sand were successively laid on the bottom of the model pool as mentioned above.
2. The soil was backfilled and compacted by layer above the coarse sand. The thickness of the layer was 5 cm. After reaching a backfilling height of 10 cm, the silo model was placed and its cylindrical wall was fixed to the overhead beam of the model pool using angle steel. Backfilling was then continued until a total height of 40 cm.
3. Balancing weight was placed at the center of the silo base, with a weight equal to the difference between the theoretical buoyancy force acting on the silo model and the self-weight of the model base.
4. Water was added to the tank, and the groundwater level was simulated by adjusting the tank height. Open the water tank valve and use a syringe to remove the air from the rubber hose. Begin recording when water seeps out from the soil surface and flows out of the outlet.
5. Maintain a constant water level in the tank. Every 30 s, slowly remove the weights from the model chamber to achieve "slow weight reducing floating" until the displacement meter reading changes abruptly. At this moment, it was considered the model bottom floats. Then closed the valve, and terminated the test.
6. The remaining weight of the counterweights inside the silo, together with the self-weight of the silo bottom, was used to calculate the buoyancy force acting on the model. This calculated value was then compared with the theoretical buoyancy for analysis.

To ensure the accuracy of experimental data, the pore water pressure transducers, miniature earth pressure cells, and displacement meters were calibrated prior to each test.

2.4 Stress analysis of underground silo

According to Archimedes principle, an object fully or partly immersed in water is subjected to a buoyancy force equal to the weight of the water displaced by the object, which can be calculated using Equation 1 as follows:

$$F_C = \rho g V \tag{1}$$

where F_c is the theoretical buoyancy force acting on the underground silo, ρ is the density of the water, g is the gravitational acceleration, and V is the volume of liquid displaced by the underground silo.

In the model test, the foundation model is partially embedded in the soil, and the force equilibrium before and after flotation can be

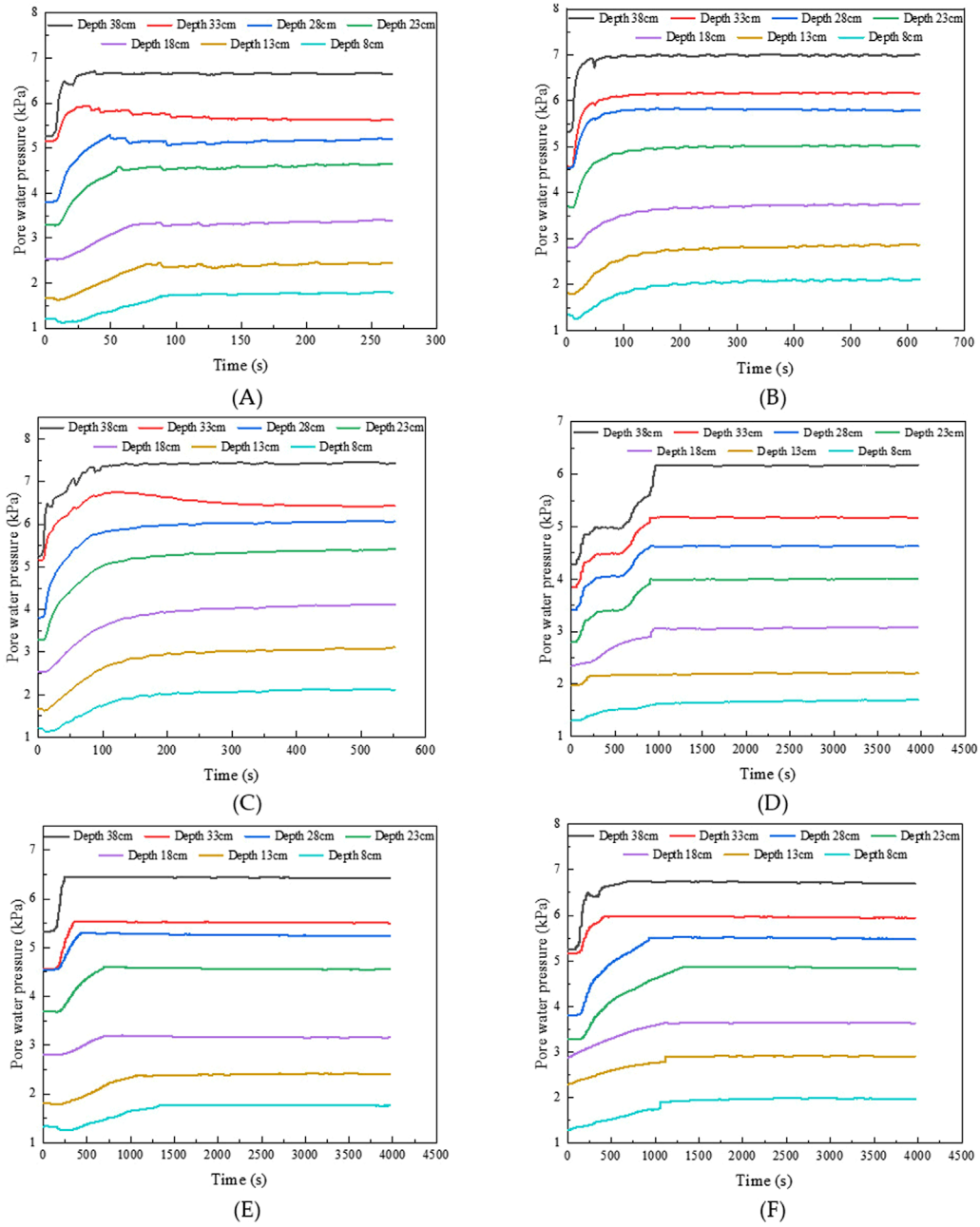

FIGURE 5
Variation of pore water pressure with time at each measurement point under different water level conditions: **(A)** S_{65}, **(B)** S_{70}, **(C)** S_{75}, **(D)** C_{65}, **(E)** C_{70}, **(F)** C_{75}.

established, as shown in Figure 4. Under static conditions, the forces acting on the model bottom can be calculated with Equation 2:

$$G = F_t + R \tag{2}$$

where G is the sum of the weight of the bottom of the underground silo and the balancing weight, F_t is the measured buoyancy force acting on the underground silo, and R is the supporting force of the bottom backfilling soil.

As previously mentioned, in this study, only the silo base uplift under the effect of water, and side friction resistance of the wall of the silo model could be neglected. When the silo model reaches the critical equilibrium state of "about to float but not yet floating," the supporting force acting on the silo base can also be considered negligible. Under these conditions, the force state of the underground silo could be expressed with Equation 3 as follows:

$$F_t = G_r \tag{3}$$

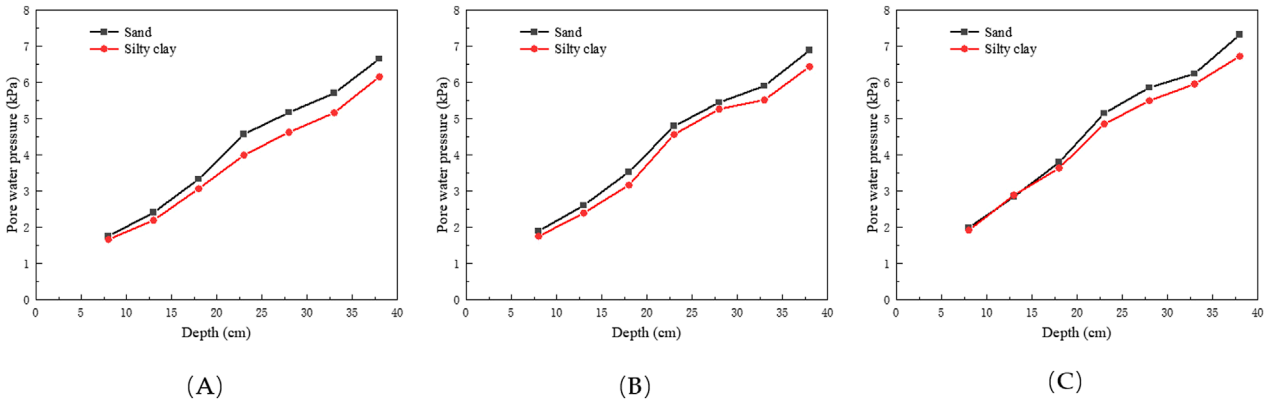

FIGURE 6
Variation patterns of pore water pressure in different soil types under the same water level: **(A)** 65 cm, **(B)** 70 cm, **(C)** 75 cm.

where F_t is the measured buoyancy force acting on the underground silo G_r is the sum of the weight of the underground silo base and the remaining balancing weight.

Based on the theoretically calculated buoyancy force, the buoyancy reduction coefficient of the silo model in different soil could be calculated using Equation 4 as follows:

$$R_s = F_t / F_c \tag{4}$$

where Rs is the buoyancy reduction coefficient of the underground silo in different soil.

The side friction resistance acting on the silo wall depends on the horizontal effective stress exerted perpendicularly on the wall and the friction coefficient between the silo wall and the surrounding soil. The side friction resistance f can be calculated using Equation 5:

$$f = l\mu \int_0^h \sigma_z' dz \tag{5}$$

where l is the perimeter of the silo wall, μ is the friction coefficient between the silo wall and the surrounding soil, h is the embedded depth of the silo wall in the soil, and σ_z' is the horizontal effective stress at the depth of z with a starting point at the surface of the backfilling soil and could be calculated using Equation 6:

$$\sigma_h' = \sigma_h - u \tag{6}$$

where σ_z is the horizontal total pressure and u is the pore water pressure at the depth of z. Since the soil used in this study is homogeneous, both σ_z and u could be considered as varying linearly with depth. These values might be obtained through linear fitting based on the measured earth pressure and pore water pressure.

3 Results and discussion

3.1 Distribution law of pore water pressure under different water levels

The variation of pore water pressure at each measurement point over time under different water level conditions in sand and silty clay are shown in Figure 5.

As shown in Figure 5, at the same water level, the time required for pore water pressure to stabilize in silty clay is significantly longer than that in sand. Moreover, at different burial depths, the pore water pressure at deeper measurement points tends to stabilize more quickly compared to those at shallower depths.

Under the same water level conditions, the stabilized pore water pressures in sand and silty clay were shown in Figure 6. Taking Figure 6A as an example, when the water level is 65 cm, the pore water pressure in sand is generally higher than that in silty clay. This is mainly attributed to the following 2 factors. On the one hand, the relative high permeability and pore connectivity of sand generally lead to fast transmission of the pore water pressure and approach to the theoretical hydrostatic water pressure (Ni et al., 2018; Yuan et al., 2025b). On the other hand, it was easy to form a micro electric field and adsorb the water molecules due to the relatively large specific surface area and the carrying of electric charges of the clay particles in the silty clay, finally building a stable diffusion double layer. In this process, both the fluidity of water molecules and the effective size of the original seepage channels were reduced, which result in lag and reduction effects in pore pressure transmission (Mitchell and Soga, 2005). Similar trends could be observed at the water levels of both 70 cm and 75 cm. On the whole, the pore water pressure at the water level of 70 cm was larger than that at the water level of 65 cm and smaller than that at the water level of 75 cm at the same depth of the same soil. Therefore, obvious influences of both the soil type and the groundwater level could be found on the transmission rate and the stabilized value of pore water pressure. Liang et al. (2024) reported that under the same water level, the pore water pressure and transmission rate in silty clay with high plasticity is lower than that in remolded loess with low plasticity. In addition,

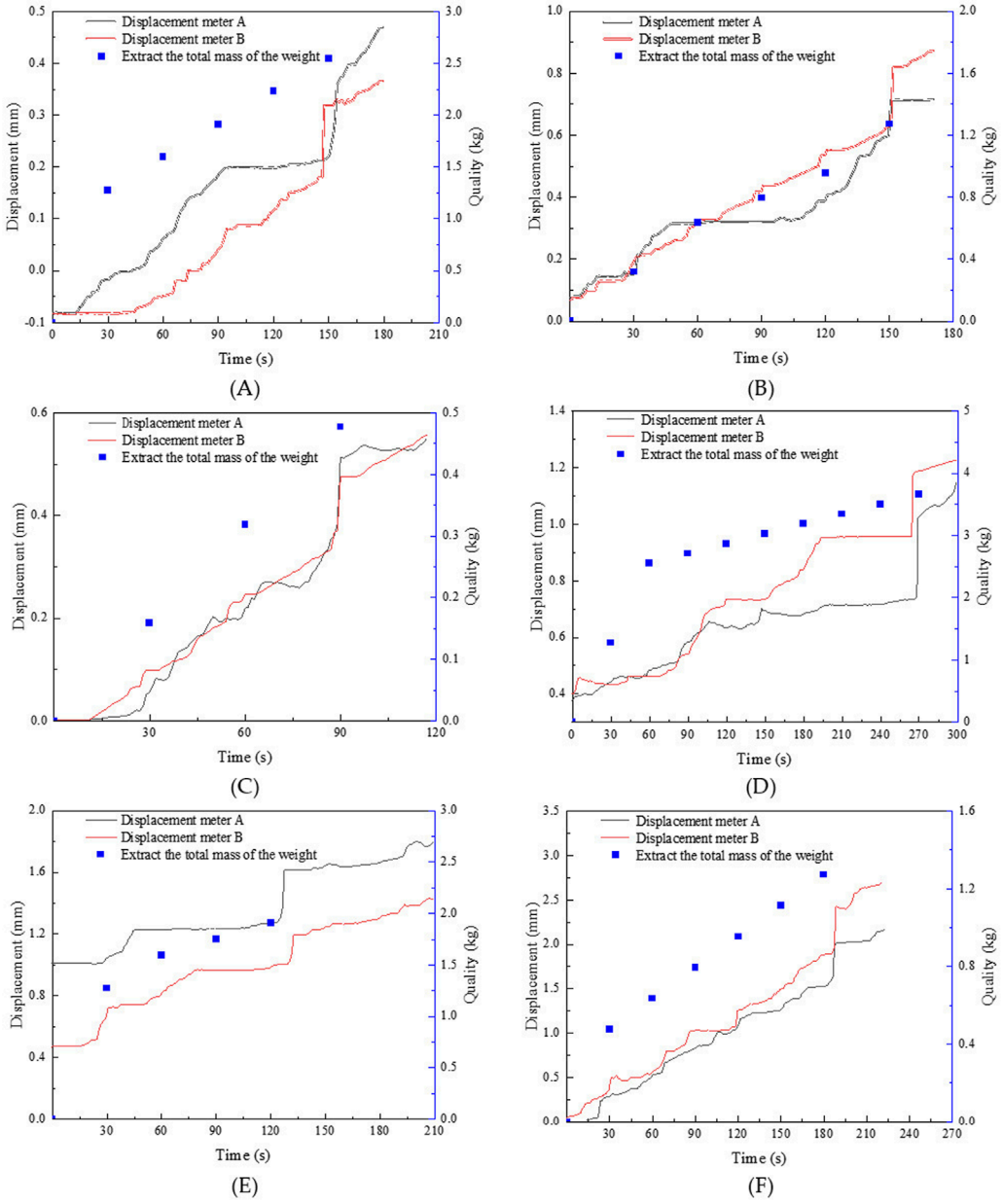

FIGURE 7
Variation of model silo displacement with time: **(A)** S_{65}, **(B)** S_{70}, **(C)** $S_{75}75$, **(D)** C_{65}, **(E)** C_{70}, **(F)** C_{75}.

obvious difference could be found in the pore water pressure in the same soil under various water levels, which is in consistent with the results in this study.

3.2 Buoyancy reduction characteristics under different water level conditions

Variations of both the displacement of the bottom of the silo model and the mass of the removed balancing weight with time of the 6 test conditions were shown in Figure 7.

During the test, as the balancing weight were gradually removed, the displacement of the model silo was observed to increase continuously. When a certain mass of balancing weight was removed, the readings of the both displacement gauges on the bottom of the silo model increased sharply at the same time. This moment was identified as the moment of model silo uplift. During the test, the mass of the removed balancing weight was recorded, and the total mass was calculated. The actual buoyancy force of the silo was calculated using Equation 3, and the results are presented in Figure 8.

The tests results indicate that, in both types of soil, the buoyancy force acting on the bottom increased significantly with the water

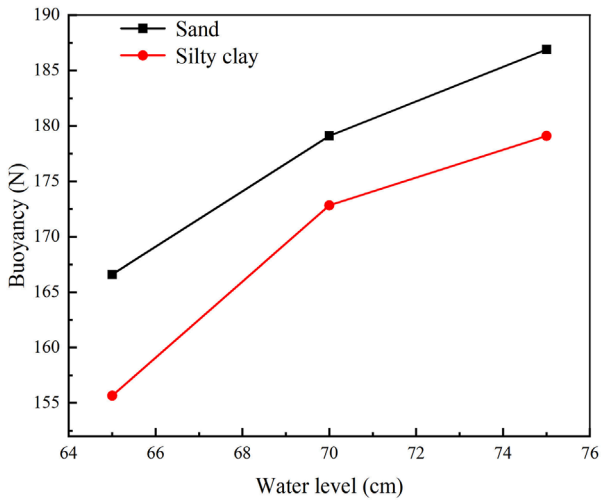

FIGURE 8
Comparison of buoyancy variation between sand and silty clay under different water levels.

level, exhibiting a well-defined linear relationship. This trend is consistent with Archimedes' principle and the mechanism of total buoyancy force increase induced by the rise of the groundwater level. Under identical water level, the buoyancy force in sand is consistently larger than that in silty clay, indicating that the soil type is of a significant influence on the transmission characteristics of buoyancy force acting on the structure. The primary reason for this difference is that sand has a relatively high porosity and permeability, and the water distribution was more homogeneous. As a result, the effective area of the structure subjected to buoyancy is relatively large, and the buoyancy effect more significant. In contrast, silty clay is characterized by small pore sizes and poor connectivity, which would result in insufficient permeability (Zhou et al., 2019). Consequently, the infiltration of the water into the pores beneath and around the structure is relatively slow within a given period of time, leading to a relatively weaker buoyancy effect. Therefore, in high water level conditions, the risk of floating for underground structures in sand is expected to large and should be given full consideration in anti-floating design.

The distribution pattern of buoyancy reduction coefficients in highly permeable soils such as sand, as presented in this study and existing literature, is shown in Figure 9A. The results indicate that in highly permeable soils represented by sand, the buoyancy reduction coefficients are generally large, with average values concentrated in the range of 0.87–0.93. The maximum values are typically close to the theoretical buoyancy (Guo et al., 2024), and the difference between the maximum and minimum values is relatively small. This indicates that the buoyancy acting on structures in such soils exhibits good stability, with the actual buoyancy closely matching the theoretical value predicted by Archimedes' principle (Mei et al., 2009; Fan et al., 2025). Therefore, the buoyancy reduction effect in sand can be considered negligible.

As shown in Figure 9B, in weakly permeability soils such as silty clay and clay, the buoyancy reduction coefficients are generally lower, with most average values ranging from 0.75 to 0.86, and some minimum values as low as 0.65. This indicates that the actual buoyancy is significantly reduced in comparison to the theoretical value. Meanwhile, the difference between the maximum and minimum values is significant, indicating considerable variability in buoyancy. This is attributed to the poor permeability and closed pore structure of silty clay, which hinder water transmission and result in actual buoyancy acting on the structure being substantially lower than the theoretical estimation. Related studies have also shown that buoyancy reduction is a common phenomenon in weakly permeability soils, and the extent of reduction is closely related to soil type, degree of compaction, and the efficiency of pore pressure transmission (Liu et al., 2024). The clay in Mei et al. (2009) and Ni et al. (2018) has a higher plasticity index, indicating a higher proportion of cohesive particles in the soil, which results in a lower reduction coefficient. In contrast, the silt clay in this study and Liang et al. (2024) has a lower plasticity index, leading to a significant difference in the reduction coefficients. The variation of the reduction coefficient should be attributed to the interaction between the buoyancy acting on the structure and the resistance provided by the soil. In anti-floating design, appropriate buoyancy reduction coefficients should be selected respectively for foundations with different soil types. In particular, for weakly permeability soils, it is recommended that a correction factor based on measured data be introduced, or that a safety factor applied, to improve the applicability and safety of anti-floating design for underground structures.

3.3 Lateral earth pressure and side friction resistance at different water levels

The total lateral pressures acting on the both sides of the silo model under different water levels and soil conditions are shown in Figure 10. Taking Figure 10A as an example, at the same burial depth conditions, the lateral earth pressure on the A and B sides of the silo are basically identical, and relatively good linear relationship between lateral earth pressure and depth could be observed. Under the all 6 test conditions, the lateral pressure acting on the silo wall basically increases linearly with depth, exhibiting a clear linear trend. This variation pattern is consistent with the classical earth and water pressure theory (Yuan B. X. et al., 2025).

Figure 11 show the average lateral pressures on the silo wall under different conditions, along with the corresponding Rankine active and passive earth pressures. The measured lateral pressure on the silo wall was between the active and passive earth pressures and close to the active earth pressure. The test results using embedded earth pressure cells on a half-scale model silo reported by Xiong et al. (2016) also confirmed that the measured lateral pressure on the silo wall at shallow depths is less than or approximately equal to the active earth pressure, which is consistent with the findings of this study.

The side friction resistance was calculated with Equation 5, and the results are shown in Figure 12. For the water levels of 65 cm, 70 cm, 75 cm, the side friction resistance acting on the underground structure were respectively 66.85 N, 61.2 N, 47.9 N in sand, and 89.7 N, 79.2 N, 64.5 N in silty clay. The side friction resistance at high

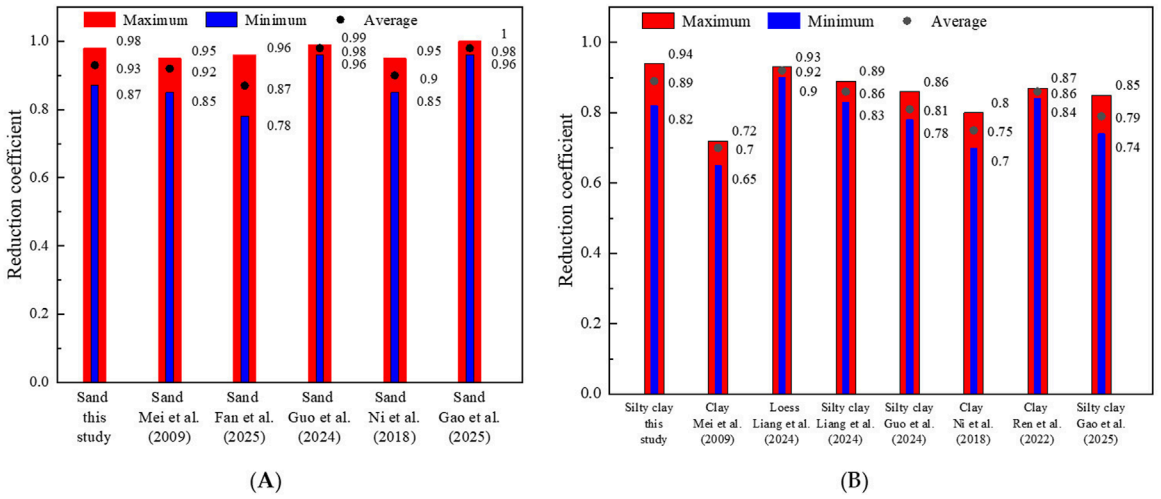

FIGURE 9
Comparison of buoyancy reduction coefficients from different studies:**(A)** Sand, **(B)** Weakly permeable soils such as silty clay and clay.

water level was obviously lower than that at low water level, both in sand and silty clay.

At high water level conditions, the pore water pressure is relatively high and the effective stress low, inducing the soil to approach a "buoyant" state. The contact between the structure and the surrounding soil was not tight, and the contribution of frictional resistance limited. At low water level conditions, the effective stress was relatively high, and the soil surrounding the structure tended to become more compacted. This enhances the friction at the soil–structure interface, leading to the more fully mobilization of the side friction resistance. Therefore, an increase in effective stress significantly enhances the normal contact force between the structure and the surrounding soil, thereby increasing the side friction resistance along the silo wall surface.

At the same water level conditions, the side friction resistance generated in silty clay is consistently larger than that in sand. This difference should be attributed to the higher cohesiveness and stronger structural adhesion of silty clay. The cohesive components significantly enhance the frictional bonding at the soil–structure interface, resulting in a more pronounced increase in side friction resistance with increasing effective stress. In contrast, sand primarily relies on internal friction. Although also affected by variations in water level, the increase in side friction resistance is relatively limited. This indicates that, due to its relatively high cohesion and fine-grained effects, silty clay is capable of providing a larger side friction resistance under practical conditions in comparison to sand.

For the water levels of 65 cm, 70 cm, 75 cm, the ratio of side friction resistance to the total buoyancy were 0.35, 0.32, and 0.25, with an average of 0.31 in sand and 0.34, 0.41, and 0.47, with an average of 0.41 in silty clay. Tang et al. (2013) found that in medium sand layers, the side friction resistance accounts for approximately 26% of the total buoyancy force. Li et al. (2020) found that the side friction resistance on a semi-underground storage tank in standard sand is approximately 22% of the theoretical buoyancy, which is similar to the results obtained from test conditions of sand in this study. Liu et al. (2021) analyzed the variation of frictional resistance on underground silos under backfilling conditions influenced by groundwater. The results show that with increasing burial depth and backfilling compaction, the side wall friction resistance increased accordingly, reaching up to 40% of the theoretical buoyancy at its maximum. The magnitude of side wall friction resistance is closely related to the soil type. Therefore, in practical engineering, the influence of soil type on the side friction resistance acting on underground structures should be properly considered in anti-floating design of underground structure.

4 Conclusion

In this study, an underground silo model was designed, and buoyancy model tests were conducted under different water level conditions in both sand and silty clay. The reduction behavior of groundwater induced buoyancy and the anti-floating contribution of side wall friction resistance were analyzed. The following conclusions were drawn:

1. At the same water level, the overall level of pore water pressure in sand is generally higher than that in silty clay, and with faster transmission and stabilization. For the same soil, the stabilization time generally decreases with the depth.
2. For the same soil, the buoyancy on the silo bottom at high water level was typically larger than that at the low water level. At identical water level, the buoyancy in sand is consistently larger than that in silty clay. At water levels of 65 cm, 70 cm, and 75 cm, the buoyancy reduction coefficients in sand are 0.87, 0.93, and 0.98, respectively, with an average of 0.93, indicating

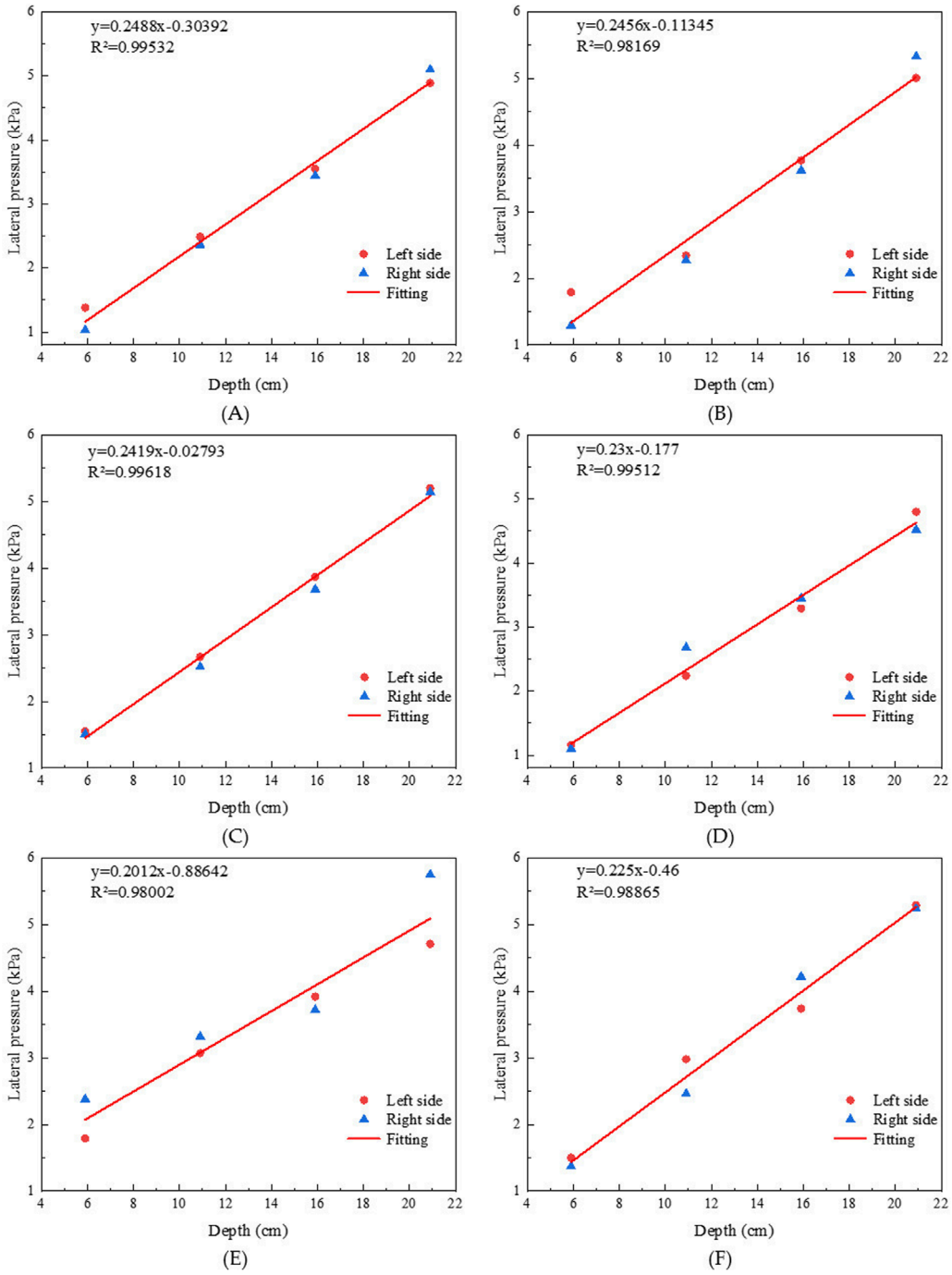

FIGURE 10
Lateral earth pressure on silo wall versus depth under different water levels: **(A)** S_{65}, **(B)** S_{70}, **(C)** S_{75}, **(D)** C_{65}, **(E)** C_{70}, **(F)** C_{75}.

that the buoyancy acting on the structure can be approximately considered unreduced. While in silty clay, the corresponding coefficients are 0.82, 0.89, and 0.94, with an average of 0.88, suggesting that the buoyancy reduction effect could not be neglected and should be corrected using measured data and empirical coefficients to ensure the reliability of the anti-floating design.

3. For the water levels of 65 cm, 70 cm, 75 cm, the side friction resistance acting on the underground structure were respectively 66.85 N, 61.2 N, 47.9 N in sand, and 89.7 N, 79.2 N, 64.5 N in silty clay. The range of the ratio of the side friction resistance to the theoretical buoyancy force was from 0.25 to 0.47, while it is often neglected or treated as a safety reserve. Thus, it is recommended that the contribution of side friction

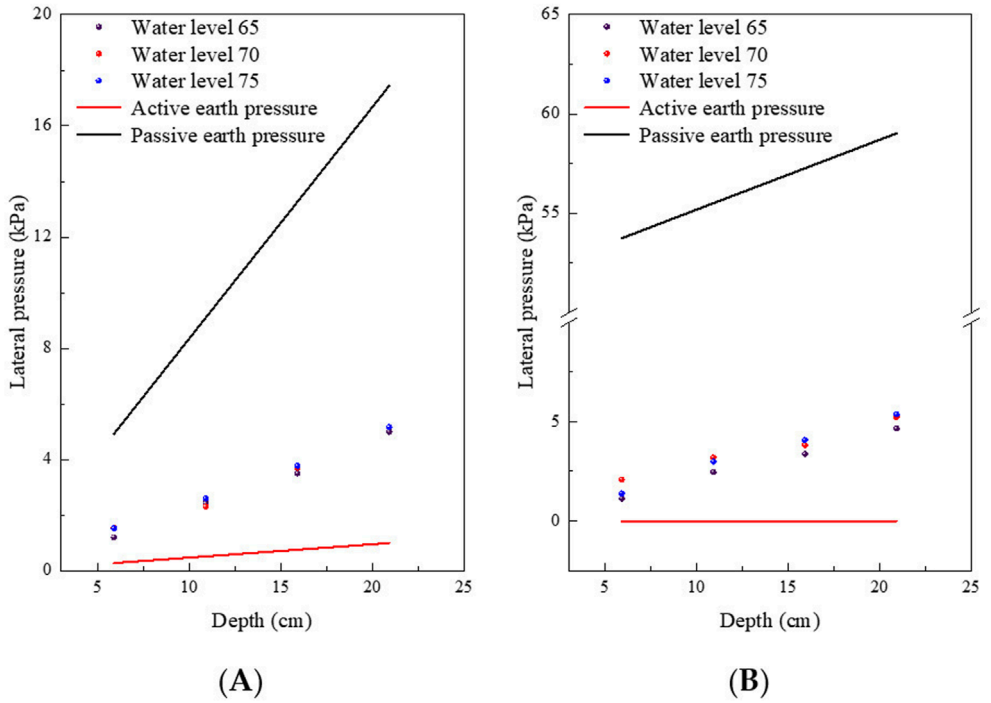

FIGURE 11
The variation of lateral pressure with depth at each point of the silo wall: **(A)** Sand, **(B)** Silty clay.

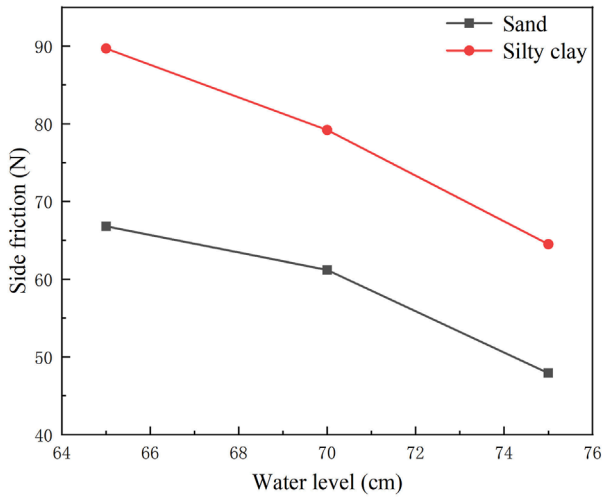

FIGURE 12
The schematic diagram of side resistance changing with water level.

resistance be properly considered in the anti-floating design in engineering practice.

Data availability statement

The original contributions presented in the study are included in the article/supplementary material, further inquiries can be directed to the corresponding author.

Author contributions

BY: Funding acquisition, Writing – review and editing, Writing – original draft, Investigation, Conceptualization. SC: Writing – review and editing, Writing – original draft, Formal Analysis, Methodology. CZ: Writing – original draft, Investigation, Formal Analysis. NS: Writing – review and editing, Supervision. SZ: Writing – review and editing, Data curation. DZ: Validation, Writing – review and editing.

Funding

The author(s) declare that financial support was received for the research and/or publication of this article. This research was funded by Henan Key Scientific and Technological Project (Grant No. 252102110373), the Open Research Subject of Henan Key Laboratory of Grain and Oil Storage Facility & Safety (Grant No. 2022KF06).

Conflict of interest

Author CZ was employed by Center International Group Co., Ltd.

The remaining authors declare that the research was conducted in the absence of any commercial or financial relationships that could be construed as a potential conflict of interest.

Generative AI statement

The author(s) declare that no Generative AI was used in the creation of this manuscript.

Any alternative text (alt text) provided alongside figures in this article has been generated by Frontiers with the support of artificial intelligence and reasonable efforts have been made to ensure accuracy, including review by the authors wherever possible. If you identify any issues, please contact us.

Publisher's note

References

Cui, Y., Cui, J., and Wu, S. (1999). Experimental study on buoyancy model tests of underground structures. *Spec. Struct.* (01), 34–37+41.

Fan, Z. S., Xu, C. J., Yang, K. L., Xue, X. L., and Zeng, C. F. (2025). Experimental study on the influence of rising water levels on the buoyancy of building structure. *Water* 17 (9), 1377. doi:10.3390/w17091377

Gao, T., Xu, Y. L., Zhou, X. M., Wang, Y. B., and Liu, H. Y. (2025). Experimental and theoretical evaluation of buoyancy reduction in saturated clay soils. *Water* 17 (12), 1832. doi:10.3390/w17121832

Guo, D., Wang, B., Tang, K., Lyu, S., Shen, C., and Xu, X. (2021). The influence of the valuing method of pile-soil friction coefficient on the simulation results of one-side excavation of bridge piles. *Highway* 66 (12), 98–106.

Guo, H. T., Zhou, R. J., Sun, C., Lin, Y. L., and Xie, J. C. (2024). Buoyancy of underground structures and pore water pressure conduction law in silty clay strata. *Heliyon* 10 (1), e24256. doi:10.1016/j.heliyon.2024.e24256

Han, X., Kong, Z., Xi, Y., and Ren, Y. (2009). The application of the improved direct shear apparatus durig research on open caisson side friction. *J. Changchun Inst. Technol. Sci. Ed.* 10 (02), 1–3. doi:10.3969/j.issn.1009-8984.2009.02.001

Hu, Y., Wan, D., and Si, Y. (2013). Anti-floating design and waterproof measures of a new type of underground grain storage warehouse. *Henan Build. Mater.* (04), 143–144. doi:10.16053/j.cnki.hnjc.2013.04.077

Jiang, M., and Guo, Z. (2017). Effects of vertical pressure and shear velocity on direct shear strength and dilatancy properties of wheat. *Trans. Chin. Soc. Agric. Eng.* 33 (06), 275–280. doi:10.11975/i.issn.1002-6819.2017.06.035

Li, K. W., Zhou, B., Xie, X. Y., Ma, X. F., and Jin, G. L. (2020). Anti-floatation design test and simulation study of large LNG underground storage tanks. *Earth Environ. Sci.* 570, 062022. doi:10.1088/1755-1315/570/6/062022

Liang, Z., Zheng, S., Liu, X., Hu, W., Du, Y., and Song, Z. (2024). Experimental study on water pressure response of underground structures in low-permeability soils. *China Civ. Eng. J.* 57 (08), 83–96. doi:10.15951/j.tmgcxb.23050373

Liu, H., and Wan, Z. (2020). Enhancement effect of base post-grouting on shaft resistance of bored piles. *Eng. J. Wuhan Univ.* 53 (12), 1078–1084. doi:10.14188/j.1671-8844.2020-12-006

Liu, H., Xu, X., Zhang, H., Wang, Z., Yang, J., and Ma, T. (2021). Friction analysis of underground silos during backfilling. *Mod. Food Sci. Technol.* 37 (06), 175–183. doi:10.13982/j.mfst.1673-9078.2021.6.1094

Liu, S. L., Sun, W. X., Zhang, W. G., Wang, Y. H., Liu, Z. C., Li, Z. C., et al. (2024). Investigation on parameters affecting reduction coefficient of groundwater buoyancy in clay layers. *J. Hydrol.* 638, 131560. doi:10.1016/j.jhydrol.2024.131560

Mei, G., Song, L., and Zai, J. (2009). Experimental study on reduction ofgroundwater buoyancy. *Chin. J. Geotechnical Eng.* 31 (09), 1476–1480. doi:10.3321/j.issn:1000-4548.2009.09.026

Mitchell, J. K., and Soga, K. (2005). *Fundamentals of soil behavior*. 3rd ed. Hoboken: John Wiley and Sons.

Mu, L., Wang, L., Huang, M., He, Y., and Kang, J. (2019). Experimental study on influences of leakage of confined water on buoyancy of underground structures. *Chin. J. Geotechnical Eng.* 41 (04), 769–774. doi:10.11779/CJGE201904022

Ni, P. P., Mei, G. X., and Zhao, Y. L. (2018). Antiflotation design for water tank using pressure relief technique. *Mar. Georesources and Geotechnol.* 36 (4), 471–483. doi:10.1080/1064119x.2017.1337255

Ren, Z. S., Lu, Q. X., Liu, K. W., Ni, P. P., and Mei, G. X. (2022). Model-scale tests to examine water pressures acting on potentially buoyant underground structures in clay strata. *J. Rock Mech. Geotech. Eng.* 14 (3), 861–872. doi:10.1016/j.jrmge.2021.09.014

Song, L., Huang, Q., Yan, D., and Mei, G. (2018). Experimental study on effect of hydraulic gradient on permeability of clay. *Chin. J. Geotechnical Eng.* 40 (09), 1635–1641. doi:10.11779/CJGE201809009

Tang, C., Xiang, W., Song, X., Zhou, M., and Jiang, P. (2013). Model test of buoyancy for underground structure in sandy-soil stratum. *J. Guangzhou Univ. Sci. Ed.* 12 (03), 34–37.

Wang, L., Xu, Q., and Liu, Y. (2013). Simple analysis of the current status and development of bulk grain building warehouses. *Grain Distrib. Technol.* (04), 9–11. doi:10.3969/j.issn.1007-3582.2013.04.004

Wang, Y., Liu, S., Shen, C., and Chen, J. (2022). Influence of contact friction on macro-micro mechanical behavior and energy evolution of granular materials. *Chin. J. Rock Mech. Eng.* 41 (02), 412–422. doi:10.13722/j.cnki.jrme.2021.0264

Xiong, X., Jin, L., and Wang, Z. (2016). Earth pressure and bearing capacity analysis on the wall of reinforced conerete underground granary. *J. Basic Sci. Eng.* 24 (01), 103–114. doi:10.16058/j.issn.1005-0930.2016.01.010

Ye, J., and Liu, G. (2010). Anti-floating safety design of structures in metro stationcon sidering friction resistance enclosure protection. *Rock Soil Mech.* 31 (S1), 279–283. doi:10.16285/j.rsm.2010.s1.014

Yuan, B., Huang, X., Huang, Q., Shiau, J., Liang, J., Zhang, B., et al. (2025a). Effects of particle size on properties of engineering muck-based geopolymers: optimization through sieving treatment. *Constr. Build. Mater* 492, 142967. doi:10.1016/j.conbuildmat.2025.142967

Yuan, B., Huang, X., Li, R., Luo, Q., Shiau, J., Wang, Y., et al. (2025b). Dynamic behavior and deformation of calcareous sand under cyclic loading. *Soil Dyn. Earthq. Eng.* 199, 109730. doi:10.1016/j.soildyn.2025.109730

Yuan, B. X., Huang, Q. Y., Xu, W. Y., Han, Z. J., Luo, Q. Z., Chen, G. R., et al. (2025c). Study on the interaction between pile and soil under lateral load in coral sand. *Geomech. Energy Environ.* 42, 100674. doi:10.1016/j.gete.2025.100674

Zhang, D. (2007). *Experimental study on anti-floating of underground structures*. Master's Thesis. Shanghai: Shanghai Jiao Tong University.

Zhang, H., Zhou, J., Chen, L., and Wang, H. (2024). Bending capacity on the bolt-weld joint in an assembled composite underground silo with steel plate and concrete. *Trans. Chin. Soc. Agric. Eng.* 40 (06), 212–219. doi:10.11975/j.issn.1002-6819.202310230

Zhang, Q., Ouyang, L., Wang, Z., Liu, H., and Zhang, Y. (2019). Buoyancy reduction coefficients for underground silos in sand and clay. *Indian Geotech. J.* 49 (2), 216–223. doi:10.1007/s40098-018-0316-4

Zhang, S., Pan, C., Wu, G., and Li, S. (2019). Study on suction of foundation in cohesive soil based on pull-out model test. *China Harb. Eng.* 39 (09), 27–31. doi:10.7640/zggwjs201909006

Zhao, Z., Zheng, S., and Jian, Y. (2022). Analysis of characteristies of sand shear strength based on taguchi method. *J. Arid Land Resour. Environ.* 36 (01), 103–110. doi:10.13448/j.cnki.jalre.2022.014

Zhou, M. (2015). Experimental study on anti-floating effect of underground structures in different soil layers. *Sichuan Cem.* (08), 70.

Zhou, J. K., Lin, C. H., Chen, C., and Zhao, X. Y. (2019). Reduction of groundwater buoyancy on the basement in weak-Permeable/Impervious foundations. *Adv. Civ. Eng.* 2019, 7826513. doi:10.1155/2019/7826513